Cell Reports, Volume *15*

Supplemental Information

High-Content Quantification of Single-Cell Immune Dynamics

Michael Junkin, Alicia J. Kaestli, Zhang Cheng, Christian Jordi, Cem Albayrak, Alexander Hoffmann, and Savaş Tay

SUPPLEMENTAL FIGURES

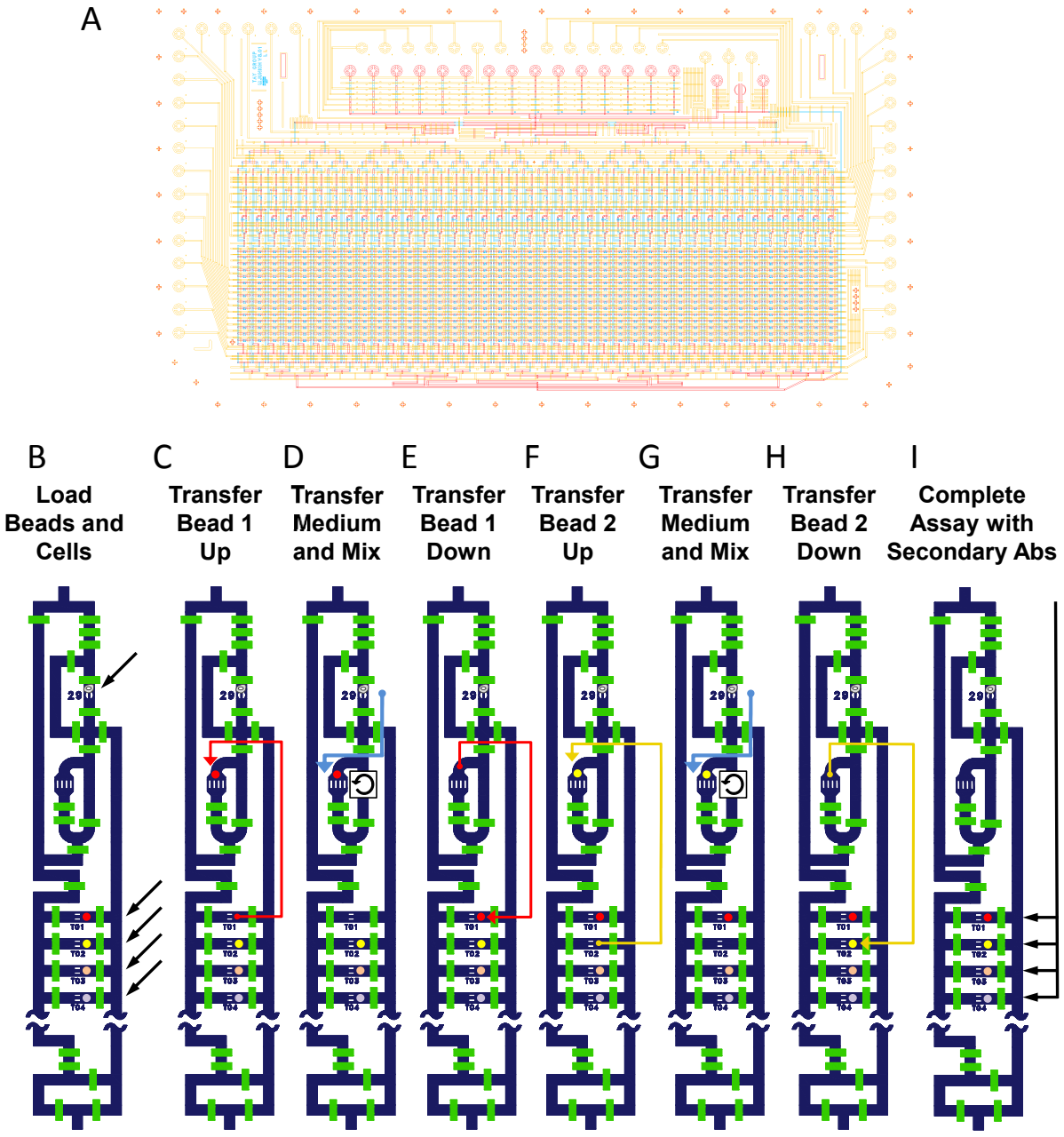

Figure S1. Design of microfluidic chip. Related to Figures 1 and 2. (A) CAD file of the overall device layout. Yellow indicates control layer, red and blue indicate the cell culture and assay layer. Functional units are arraigned in isolated columns. See (Figure 1) and text for details of individual components. (B-I) Diagram of assay operation. (B) Cells and beads are directed into desired chambers by valves and retained by traps or weirs. (C) On-chip peristaltic pumps are used to transfer beads from Bead Storage Chambers to Binding Chambers. (D) Medium is

transferred from Cell Chambers to Binding Chambers and mixed with another on-chip peristaltic pump to bind secreted molecules to antibody functionalized beads. (E) After sufficient mixing time for binding, beads are transferred back to Bead Storage Chambers with flow. During this transfer, the bead is also rinsed. (F-H) The cycle repeats for following time point measurements with the next beads from subsequent Bead Storage Chambers. (I) After all medium measurements are finished, beads are exposed to secondary antibodies to complete the sandwich immune assay and imaged. The chip is comprised of 40 such columns operating in parallel, however each of the 40 columns is individually addressable with an inlet binary tree multiplexer (not shown).

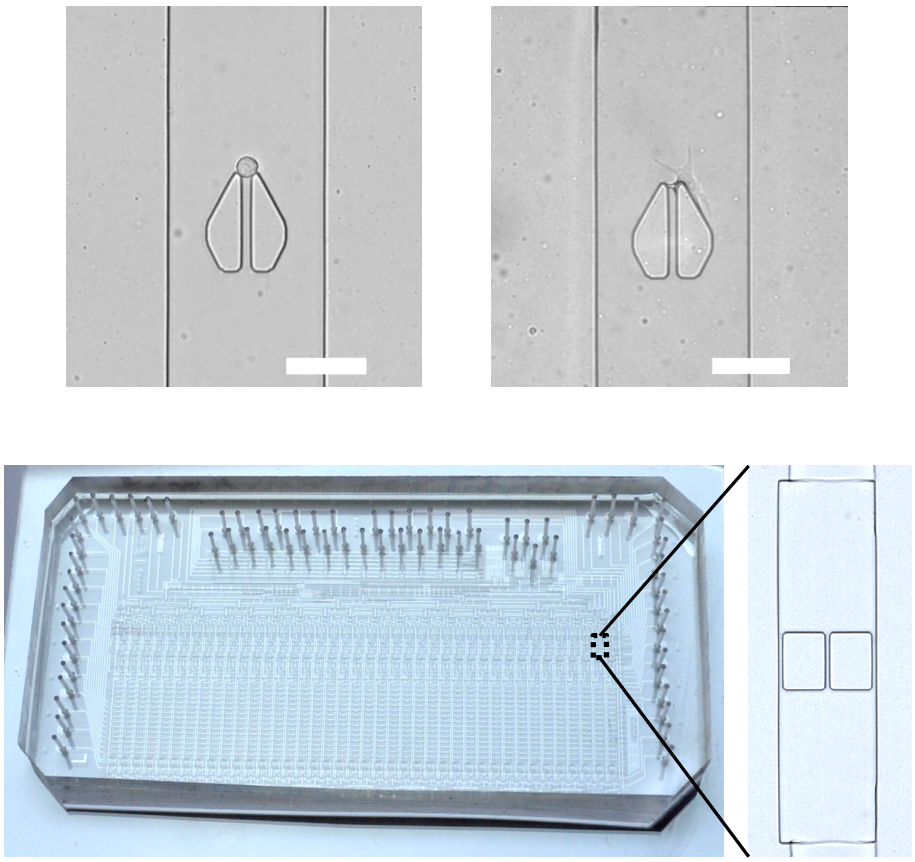

Figure S2. Cell trapping and retention. Related to Section: Capture and culture of isolated single-cells and Figure 1. (Top Left) A cell immediately after being retained by the fluidic trap for adherent cells. Fluid flow holds the cell against the trap structure while excess cells pass through the trap area, see also (**Supplemental Video 1**). (Top Right) Cells attached shortly (~5 minutes) after being retained by fluidic traps. Once attached, cells can be washed, supplied medium and stimulated while remaining inside individual chambers. Scale bar is 50 μm. (Bottom) Chip design for non-adherent and rare cell populations. Overall chip architecture is similar to that for non-adherent cells except for trap design shown at right which captures all objects introduced into cell chamber. Traps are placed inside chambers which can be opened and closed via valves so that the cellular environment can be isolated and sampled for measurement at defined times.

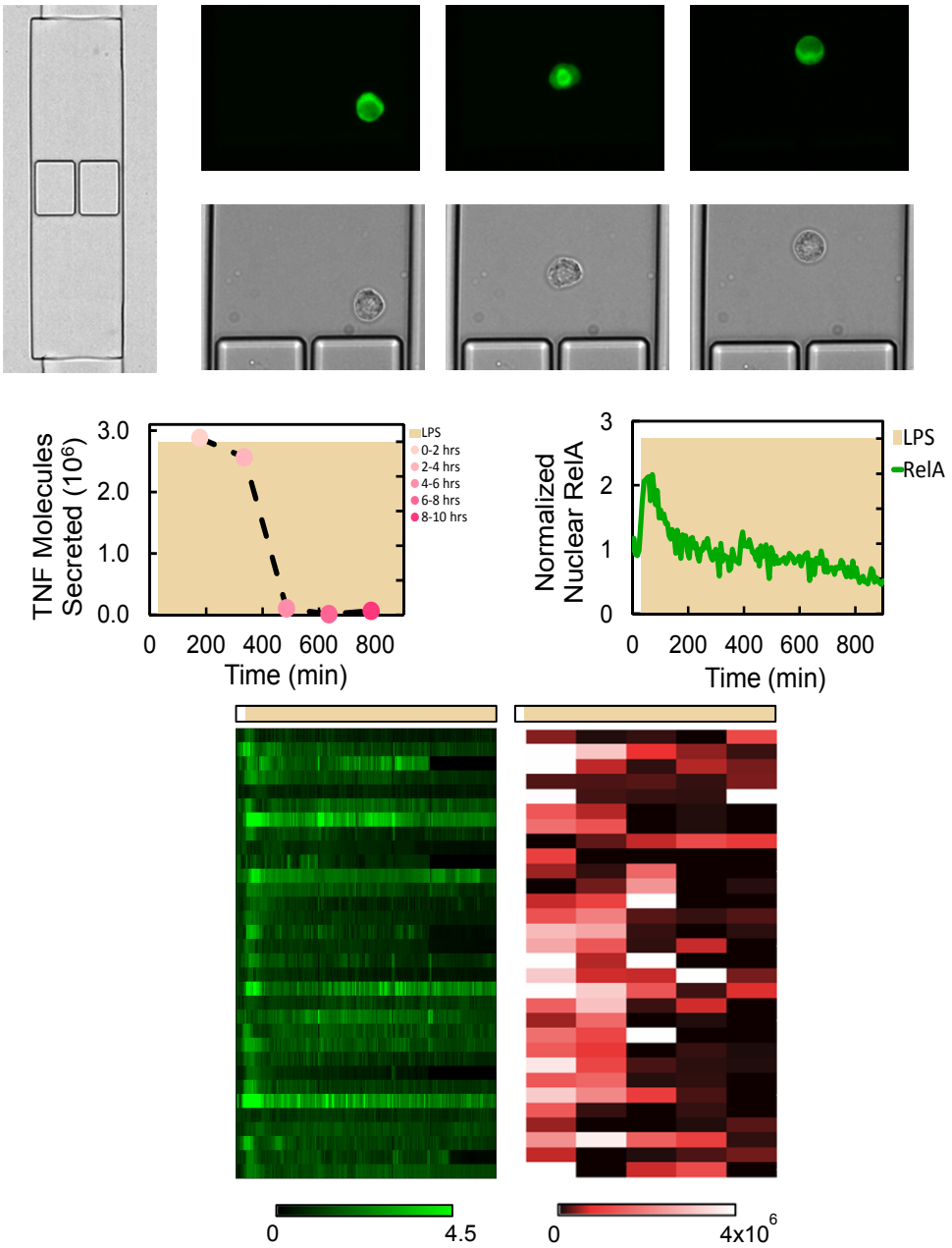

Figure S3. Measurement of suspension cells. Related to Section: Capture and culture of isolated single-cells and Figures 1 and 4. Weir type trap design (top left) was used to isolate RAW macrophages inside channels functionalized to be non-adherent. Image sequence shows RelA activity and brightfield monitoring for same cells. Middle panels display measurement of TNF and RelA traces for a single cell stimulated with LPS (500 ng ml^{-1}). Lower heatmaps display 10 hours of RelA (left) and TNF (right) data from a population of single macrophages measured in suspension on chip.

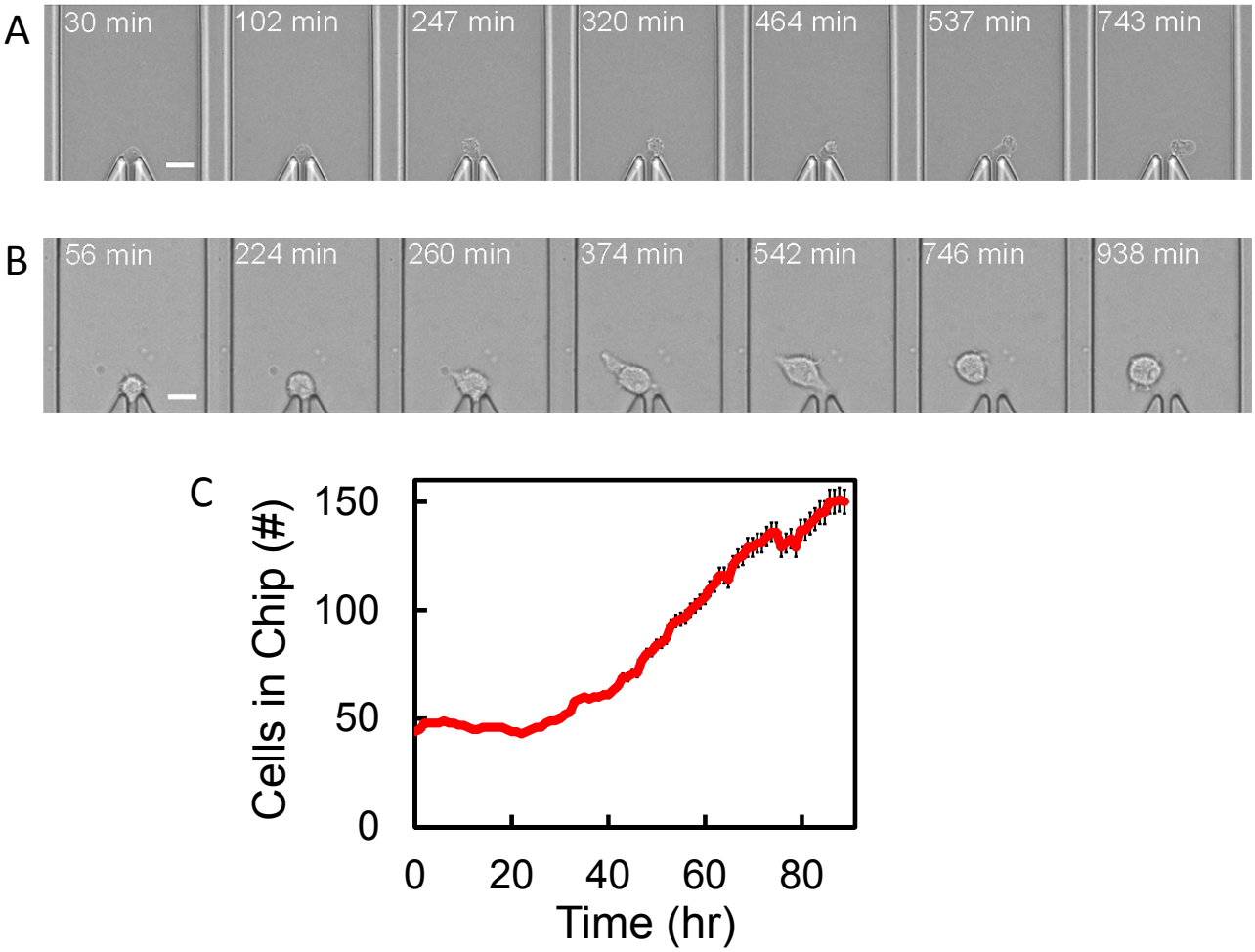

Figure S4. Critical parameters for single-cell culture. Related to Section: Capture and culture of isolated single-cells and Figures 1 and 4. (A) Culture of single cells without sufficient humidity control or rinsing of Pluronic. Incorrect culture parameters results in poor attachment, unhealthy cells and early cell death. (B) Culture of single cells under optimized conditions. Cells rapidly attach and can be maintained for several days of experimentation. Times indicate minutes since seeding. Scale bars are 20 μm. (C) Representative measure of on-chip cell viability. RAW 264.7 macrophages were seeded into cell chambers and supplied with fresh medium every two hours. Line indicates total number of cells inside the microfluidic device. Error bars show standard deviation of cell number per chamber

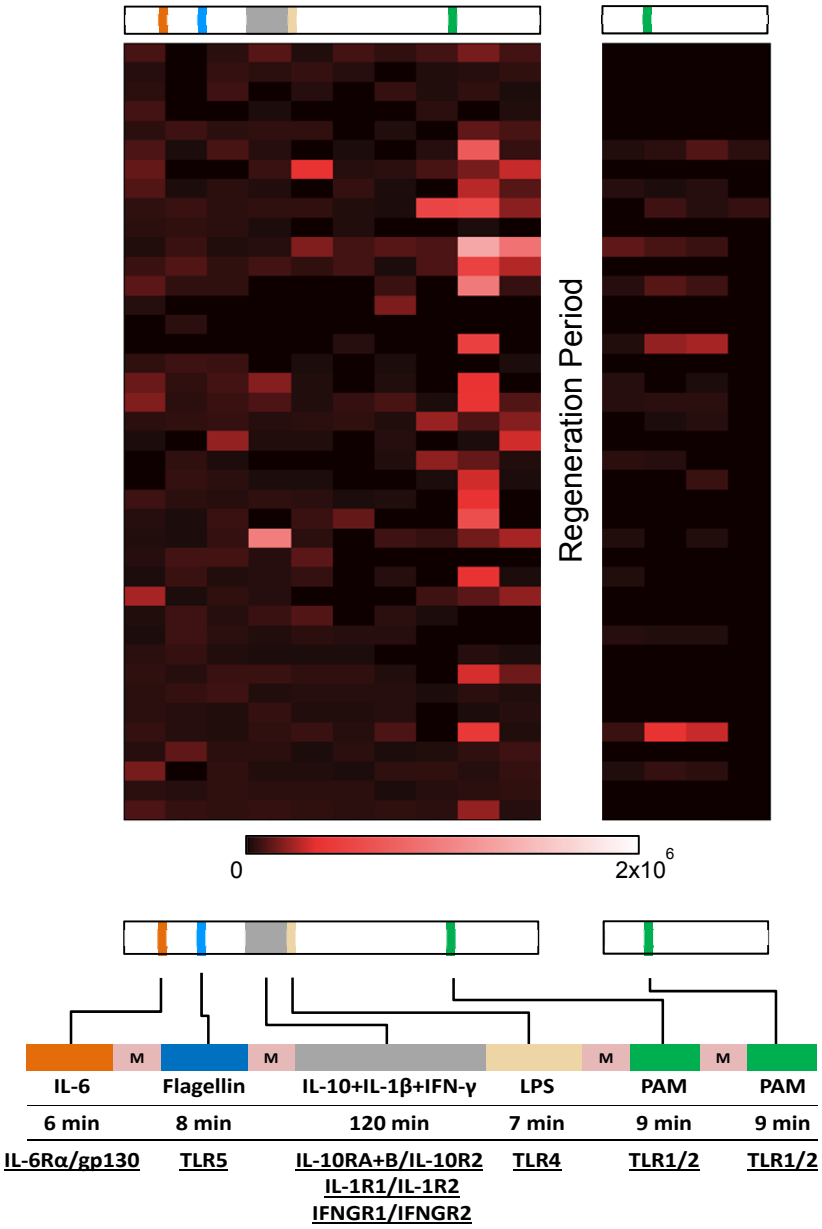

Figure S5. Supply of complex, dynamic immune inputs. Related to Section: Automated generation of dynamic and complex signaling inputs and Figure 4. Heatmap shows TNF secretion data for cells stimulated with a range of immune inputs. Lower diagram depicts ligands supplied along with their time courses and corresponding receptors for each ligand.

System Parameter	Capability
STIMULATION	
Resolution	Seconds - hours
Number of inputs or doses	15
Control	Fully automatic
MEASUREMENT	
Resolution *(Secretion)*	Minutes – hours
Multiplexing *(# of Cytokines / molecules)*	~10
Total number of measurements *(Secretion)*	>15 x Number of cytokines*
Resolution *(Imaging of fusion proteins, migration, morphology*	Minutes
Total number of measurements *(Imaging)*	6 channels
Control	Fully automatic
CELL CULTURE	
Number of single cells	40
Culture duration	Days - Week
Control	Fully automatic

***** Chip can be reloaded with additional beads during experiments

Figure S6. Stimulation, measurement, and culture capabilities of the microfluidic system enabled by the combination of the chip design and system automation. Related to Section: Automated live cell culture and microscopy and Figures 3 and 4.

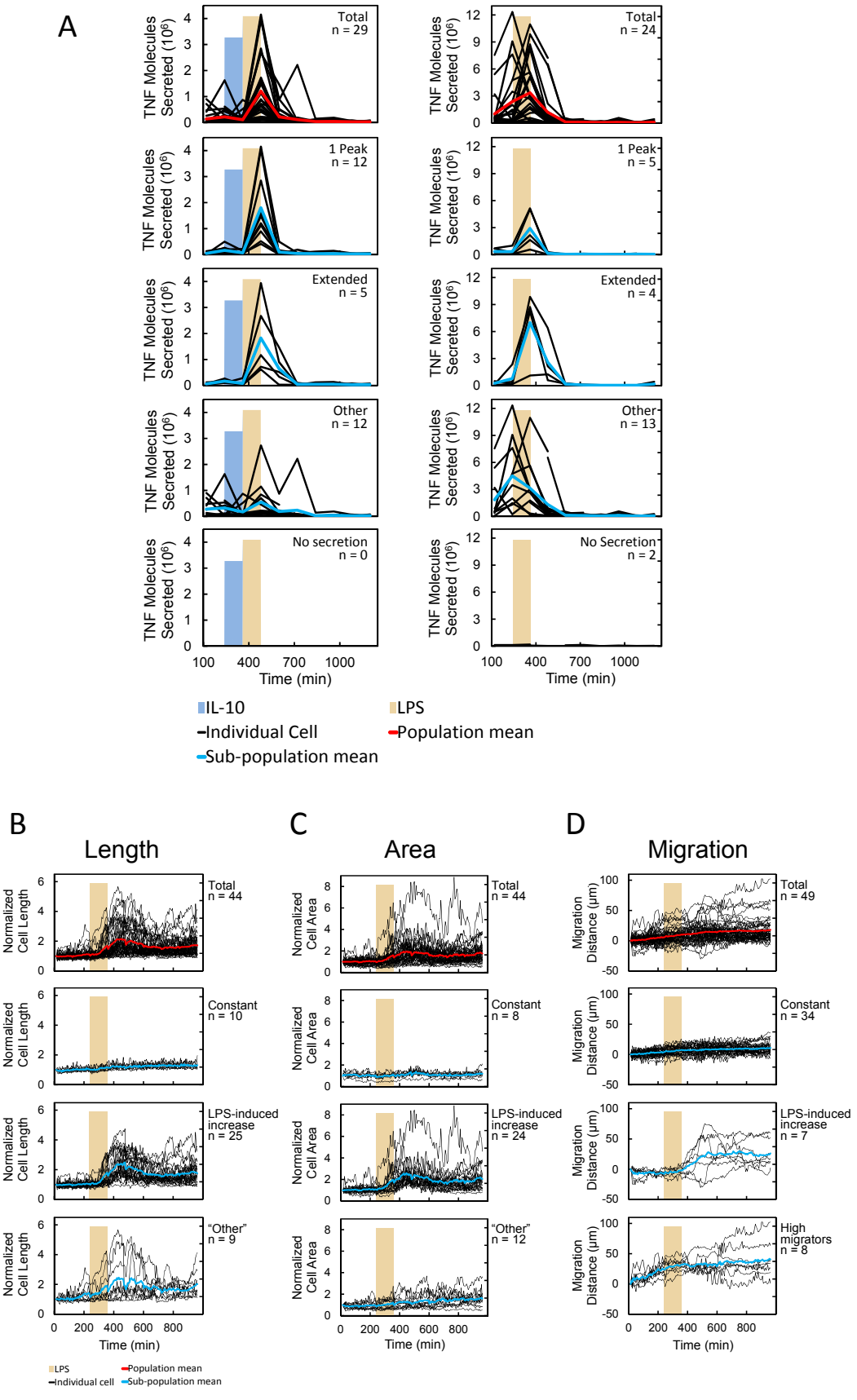
A
TNF Molecules Secreted (10^6)
Total
n = 29
Total
n = 24
1 Peak
n = 12
1 Peak
n = 5
Extended
n = 5
Extended
n = 4
Other
n = 12
Other
n = 13
No secretion
n = 0
No Secretion
n = 2
100 400 700 1000
Time (min)
IL-10
LPS
Individual Cell
Population mean
Sub-population mean
B
Length
C
Area
D
Migration
Normalized Cell Length
Normalized Cell Area
Migration Distance (μm)
Total
n = 44
Total
n = 49
Constant
n = 10
Constant
n = 8
Constant
n = 34
LPS-induced increase
n = 25
LPS-induced increase
n = 24
LPS-induced increase
n = 7
"Other"
n = 9
"Other"
n = 12
High migrators
n = 8
0 200 400 600 800
Time (min)
LPS
Population mean
Individual cell
Sub-population mean

Figure S7. Additional macrophage measurements. Related to Figure 5. (A) Heterogeneity in single-cell immune TNF dynamics in response to two hours of IL-10 (20 ng ml^{-1}) (blue) followed by two hours of LPS (500 ng ml^{-1}) (tan), or two hours of LPS. The graphs depict whole population and subpopulation responses from top to bottom respectively. (B-D) Migration and morphological data for two hour high dose LPS stimulation from cells from a single chip. Related to Section: Multiparameter analysis of single immune cells reveals poorly correlated NF-κB and TNF secretion dynamics. (B) Length, (C) Cell area. (D) Migration. Each behavior possesses subpopulations with distinct phenotypes. The subpopulation do not correlate to each other with the exception of length and area.

SUPPLEMENTAL VIDEOS

Video 1: Cell Capture, Related to Figure 1

Video 2: Rapid Stimulation, Related to Figure 4

Video 3: Bead Transferring, Related to Figure1

Video 4: Medium Transfer, Related to Figure 1, Related to Figure 1

Video 5: Rapid Mixing Inside Assay Chambers, Related to Figure 2

Video 6: Mixing During Binding to Bead Surface, Related to Figure 2

Video 7: Fluid Movement Across a Retained Non-adherent Cell, Related to Figure 1

SUPPLEMENTAL EXPERIMENTAL PROCEDURES

Fabrication of master molds for PDMS casting

Molds for microfluidic flow layers for chips were created by spinning AZ50XT (AZ Electronic Materials) resist onto silicon wafers to a height of 23 μm. This resist was then patterned with a polyester film mask from (International Phototool Company, Colorado Springs, CO USA) before being heated to reflow or round its profile. SU8-3025 (MicroChem) was then spun onto the wafers to a height of 25 μm and patterned by a chrome mask obtained from (Delta Mask, Enschede, The Netherlands) using an I-line filter. SU8-3025 was also patterned to a height of 25 μm for control molds using a polyester film mask. Molds were then hardbaked and coated with TMCS (Sigma-Aldrich, 448931) under a fume hood to prevent PDMS sticking to the molds. Detailed protocols are available upon request.

PDMS for microfluidic chips (RTV615, Momentive Performance Materials) was used at a 10:1 ratio. The PDMS was cast to a height of 6 mm for flow layers and spun at 2600 RPM for control layers with a spincoater (Spin150, SPS-Europe, Putten, The Netherlands). Holes for supply and control inputs were punched with a 0.89 mm diameter punch (SYNEO, Schmidt Catheter punch). Flow layers were cleaned with tape (3M Scot MagicTM) before being oxygen plasma activated at 20 Watts for 15 seconds in a plasma machine (Diener, Femto, Ebhausen Germany). The two layers were then aligned with a stereo microscope (Nikon SMZ 1500) equipped with two X-Y stages, and immediately placed in an 80°C oven. Chips were kept in the oven for 7 days prior to autoclaving at 121°C for 30 minutes. Post autoclaving, chips were dried at 80°C for 2 hours before use as described above. Detailed protocols are available upon request.

Off-chip cell culture

Macrophages (RAW 264.7) were maintained off chip in non-tissue culture treated T75 flasks (Greiner Bio-One, 658195), and were passaged every three days using versene (Life Technologies, 15040-033). Medium for macrophages consisted of DMEM, (Sigma Aldrich, D6429) with 10 % FBS (Sigma Aldrich, F9665), 1% GlutaMax (Life Technologies, 35050-038), and 2% HEPES (Life Technologies, 15630-056). Jurkat cells were maintained off chip in non-tissue culture treated T75 flasks (Greiner Bio-One, 658195), and were passaged every three days. Medium for Jurkats consisted of RPMI, (Life Technologies, 52400-025) with 10 % heat inactivated FBS (Sigma Aldrich, F9665), 1% GlutaMax (Life Technologies, A12860-01), 1% non essential amino acids (Life Technologies, 11140-035), and 0.2% Penicillin-Streptomycin (Life Technologies 15140-122). 3T3 cells were maintained off chip in tissue culture treated T75 flasks (Greiner Bio-One, 658175), and were passaged every three days. Medium for 3T3 cells consisted of DMEM, (Life Technologies, 41965-062) with 10 % FBS (Sigma Aldrich, F9665), 1% GlutaMax (Life Technologies, 35050-038), and 1% Penicillin-Streptomycin (Life Technologies 15140-122). KL25 cells were maintained off chip in Nunclon Delta-treated T25 flasks (Thermo Scientific, 156367), and were passaged every two to three days. Medium for KL25 cells was made of DMEM (Life Technologies, 11960-044), 10% FBS (Sigma Aldrich, F9665), 10 mM Hepes (Life Technologies, 15630-056), 0.2% Penicillin-Streptomycin (Life

Technologies 15140-122), 2 mM L-Glutamine (Life Technologies, 25030-032), and 50 uM 2 Mercaptoethanol (Sigma Aldrich, M3148). Normal medium for each cell type was used for on-chip culture and experiments. Macrophages (Wall et al., 2009) were obtained from the Ian Fraser Lab, NIH USA, Jurkat cells were obtained from the Christoph Hess, University of Basel, Switzerland. 3T3 cells (Lee et al., 2009) were obtained from the Quake Lab, Stanford University, USA, and KL-25 (Bruns et al., 1983) cells were obtained from the Reddy Lab, ETH Zürich.

Assay components for on chip cellular staining

Components for on-chip cell staining included BD Cytofix/Cytoperm, (BD Biosciences 554722) for cell fixation and permeabilization, and ActinRed 555 ReadyProbes reagent (Life Technologies R37112) for actin labeling. Cells were staining by flowing the fixing and permeabilization solution over cells for five minutes, followed by ten minutes of flow of the actin staining solution diluted to one drop ml^{-1} of medium, and finally ten minutes of flow with PBS before imaging. All steps were undertaken under standard cell culture conditions (37ºC, saturating humidity and a 5% CO_2 atmosphere).

Statistical analysis of data

Statistical analysis of the data presented is as follows. For calibration curves, the sample size was selected to ensure adjacent calibration values could be distinguished reliably given noise levels (i.e. $P \leq 0.01$ using a two-tailed, unequal variance t-test). For data shown in Figure 4B, Figure S3, and Figure S6 heatmaps include all measurements gathered from chip experiments including when multiple cells were present inside a chamber. Numbers are 40 chambers for single two hour pulse, repeated pulses of LPS and multiparameter stimulation, and 24 chambers for constant LPS exposure. Only single cell time courses were used for subsequent comparisons with the exception of modeling where averages of RelA profiles and summed TNF released from multiple cells in a single chamber were considered. For analysis of mRNA transcript number, outliers were classified using a local outlier factor (LOF) which calculates the densities of measurements around each data point (Breunig et al., 2000). With this classification, outliers or sub-clusters differ from the bulk data in their local measurement density. Using a five nearest neighbors approach to calculate the LOF we classified two *CD147* measurements (90.6, 111) as outliers and for *Gapdh*, we identified five measurements that formed a sub-cluster separated from the other data points (34.8, 428, 478, 536 and 1204) which were subsequently removed from further analysis. The remaining data were fit to gamma distributions and the Kolmogorov-Smirnov (KS) and the more powerful Anderson-Darling (AD) tests were used as goodness of fit measures (Stephens, 1974). The generated p-Values (KS: 0.92, AD: 0.85 for *CD147*, and KS: 0.83, AD: 0.85 for *Gapdh*) revealed no significant difference between the distributions of measured mRNA values and the fitted gamma distribution.

Mathematical modeling of dynamic RelA and TNF

Previous TLR4-TNF modeling efforts have been used to study bulk-measurement-based TNF production under different knockout conditions (e.g. wild-type, TRIF-/- and MYD88-/-) and thus were developed as deterministic

models without consideration of cell-to-cell variability (Caldwell et al., 2014), rendering them incapable for studying single-cell behavior. Subsequent to this, the extrinsic noise related to TLR4 signaling has been characterized, and it has been determined that by introducing log-normally distributed TLR4 generation, MyD88 and TRIF activation, together with an experimentally measured Gaussian distribution of the endosome maturation time, the TLR4 model can explain single-cell reactions for different doses of LPS stimulation (Cheng et al., 2015). These details have been incorporated in the current study, updating the TLR4 model from (Cheng et al., 2015) to be able to simulate single-cell behavior.

Another modification relates to the fact that the original model takes NF-κB as an input, constituting of genotype-dependent (mainly TRIF-dependent) rates of transcription, mRNA processing, mRNA degradation, translation and secretion (Caldwell et al., 2014). Here, however, the TRIF-regulation was changed from a genotype-dependent multiplier into a regulation function, to better reflect actual regulation. Specifically, there are four places of TRIF regulation: A function of stimulus-responsive control of processing (kpr), half-life control (degradation rate kdegm), translation (ktl), pro-protein processing and secretion (ksec), included in the model as shown below:

$$k_{pr} = k_{pr0} * f_a\,(TRIF(t))$$

$$k_{degm} = k_{degm0} * f_i\,(TRIF(t))$$

$$k_{tl} = k_{tl0} * f_a\,(TRIF(t))$$

$$k_{sec} = k_{sec0} * f_a\,(TRIF(t))$$

with regulation as the following:

$$f_a(TRIF(t)) = \frac{TRIF(t) + K_{a0}}{TRIF(t) + K_a}$$

$$f_i(TRIF(t)) = \frac{K_i}{TRIF(t) + K_i}$$

Please see original manuscripts for further code details (Cheng et al., 2015, Caldwell et al., 2014).

Random walk model for protein diffusion and capture

A 2D random walk model was implemented in MATLAB to simulate capture of cytokines on beads inside a microchannel environment. The model was formulated as follows. A chamber was defined as a rectangular shape having similar dimensions to the actual microfluidic device. Particles having no dimension and no interactions with each other representing cytokines were then randomly distributed within the chamber and a region the size of an antibody functionalized bead, representing the capture, surface was established within the box. In the case of diffusive transfer, during each one second time step of the simulation, particles were given a randomly oriented displacement and moved a fixed distance on this trajectory. The distance traveled was calculated from the diffusion constant of the given cytokine. In the case of mixing, particles locations were randomized at each time step to mimic

the high convective transfer provided by on chip peristaltic mixing. If a particle travelled outside of the defined chamber, it was considered as reflected off the chamber wall and resumed its previous position. If a particle entered the capture area, it was treated as bound to the bead and removed from further diffusive movement. The output of movements and capture were then displayed graphically, Figure 2D, and the number of captured cytokines was plotted at certain times. The effects of various parameters upon capture were explored including the presence and absence of mixing, altered channel dimensions, and different diffusion coefficients corresponding to different cytokines. Code is available upon request.

Multiplexed on-chip measurements of single-cell secreted cytokines

Multicomponent outputs are part of any immune response and their functions can be explored by examining release of multiple cytokines via utilizing the multiplexing capability of the system. To this end, detection of secreted cytokines from macrophage medium for TNF, IL-6, IL-10, IL-12, IFN-γ, and MCP-1 has been performed. These beads (except for TNF) originated from kits (see above) encoding cytokine identity via tagging for a particular antibody with an internal dye, and allow simultaneous detection of a highly flexible number of components in one sample (Figure 3A). As with the previous experiments, the secretion data was coupled with the known input dynamics, which for this scenario consisted of continuous LPS exposure (500 ng ml^{-1}), as well as the internal NF-κB reaction, and migration and morphology data.

Effect of complex, dynamic input history on TNF secretion from single cells

Complex, multidimensional signal histories exist during the course of an immune reaction, though what their effects may be upon immune cell functions and even their specific compositions remain largely unexplored. As an initial exploration of this aspect of immunity, additional immune scenarios were tested via the device to probe various temporal, signal history, and multiparameter effects upon immune input-output relationships. We provided cells an input history over more than two days consisting of typical pro- and anti-inflammatory stimuli at different time scales, ranging from cytokines to various pathogen-based ligands. TNF secretion dynamics, NF-κB and migration and morphology were again measured. The stimuli duration ranged from as short as seven minutes, to longer inputs of two hours, (Figure S6). IL-6 with known anti-inflammatory properties (Starkie et al., 2003) was first briefly supplied followed by short exposure to flagellin, then a mixture of the cytokines IL-10, IL-1β, IFN-γ for two hours before an immediate short exposure to a low dose of LPS. Cells were then supplied with medium for eight hours before being exposed to a brief pulse of bacterial Pam3CSK4. They were then allowed to recover for 34 hours, before the chip was reloaded with additional beads and an identical pulse of Pam3CSK4 was again given, simulating re-exposure to the pathogen. During this long-term complex input delivery, the cells were measured in all three modes (TNF secretion, NF-κB and migration). These measurements demonstrate firstly the comprehensive ability to supply long-term inputs at rapid and varying timescales as well as the dependence of the cellular history on its ultimate response. We observed that the stimulations prior to administration of LPS rendered cells refractive to this stimulant, in terms of both NF-κB activation and TNF release as they would normally respond to the supplied dose, (Figure S6). This single experiment generated an extensive multiparameter, data set and demonstrated several days of automated culture and experimentation with a complex input history. Though the shortest pulse of stimulant

given was seven minutes, inputs as short as several seconds can also be applied to cells, as time-pulses are limited only by valve openings which take place in the sub-second range, (Supplemental Video 2).

End point measurements of single-cells: on-chip immunostaining, harvesting for clonal expansion, and gene expression

Single cells have been stained on the chip for key proteins via automatic delivery of staining components (see above), (Figure 3B), and been harvested via flowing out of the chip into individual wells of a 96 well plate. Single-cell harvesting allows for either expansion of these cells, (Figure 3C), which enables a number of uses such as enriching for certain populations, or allows for directly analyzing gene expression of single-cells. We have retrieved single cells from the chip and measured absolute mRNA transcript numbers via droplet digital PCR (see Experimental Procedures) for several genes (both lowly and highly expressed) in different cell types as a proof of this concept, (Figure 3D). Measuring cells retrieved from the chip, we found that both *Gapdh* and *CD147* mRNA copy numbers in single mouse macrophages are highly variable. The measured single-cell mRNA distributions are super-Poisson, and fit well to a gamma distribution, (see below), supporting a stochastic two-state (random telegraph) model for gene expression in these cells. From the measured gamma distributions, a burst size per gene activation of 25±9 for *CD147*, and 313±92 mRNAs for *Gapdh* were calculated, and bursting frequencies of 0.69±0.19 per day for *CD147*, and 19.1±5.5 per day for *Gapdh* were derived based on published values of mRNA half-lives (Schwanhäusser et al., 2011, Kuwano et al., 2009).

Analysis of single-cell mRNA measurements

The measured mRNA copy numbers were fit to several possible probability density functions (pdf's) to determine their most likely distribution. As the variance of the observed data is much higher than their mean, the poisson pdf is not a good fit ($p << 0.05$ $\chi 2$-test). The gamma pdf, conversely, satisfactorily reproduces both the *CD147* and *Gapdh* mRNA copy number distributions. These findings agree with a two state model of gene expression, where a gene can switch between phases of transcription and inactivity (Paulsson, 2005, Peccoud and Ycart, 1995, Raj and van Oudenaarden, 2008). These oscillations lead to an increased copy number variance compared to a case of constant mRNA production and degradation. Furthermore, it has been shown previously, that the shape and rate parameters of the fitted gamma distribution are indicators of the bursting rate of a gene (how often the gene is actively transcribed) and its burst size (how many transcripts are on average produced per period of activity) (Raj et al., 2006, Cai et al., 2006, Schwanhäusser et al., 2011, Kuwano et al., 2009).

Supplemental References

Breunig, M. M., Kriegel, H.-P., Ng, R. T. & Sander, J. 2000. LOF: identifying density-based local outliers. *SIGMOD Rec.,* 29**,** 93-104.

Bruns, M., Cihak, J., Müller, G. & Lehmann-Grube, F. 1983. Lymphocytic choriomeningitis virus. VI. Isolation of a glycoprotein mediating neutralization. *Virology,* 130**,** 247-251.

Cai, L., Friedman, N. & Xie, X. S. 2006. Stochastic protein expression in individual cells at the single molecule level. *Nature,* 440**,** 358-362.

Caldwell, A. B., Cheng, Z., Vargas, J. D., Birnbaum, H. A. & Hoffmann, A. 2014. Network dynamics determine the autocrine and paracrine signaling functions of TNF. *Genes & Development,* 28**,** 2120-2133.

Cheng, Z., Taylor, B., Ourthiague, D. R. & Hoffmann, A. 2015. Distinct single-cell signaling characteristics are conferred by the MyD88 and TRIF pathways during TLR4 activation. *Sci. Signal.,* 8**,** ra69-ra69.

Kuwano, Y., Rabinovic, A., Srikantan, S., Gorospe, M. & Demple, B. 2009. Analysis of Nitric Oxide-Stabilized mRNAs in Human Fibroblasts Reveals HuR-Dependent Heme Oxygenase 1 Upregulation. *Molecular and Cellular Biology,* 29**,** 2622-2635.

Lee, T. K., Denny, E. M., Sanghvi, J. C., Gaston, J. E., Maynard, N. D., Hughey, J. J. & Covert, M. W. 2009. A Noisy Paracrine Signal Determines the Cellular NF-kB Response to Lipopolysaccharide. *Sci. Signal.,* 2**,** ra65-.

Paulsson, J. 2005. Models of stochastic gene expression. *Physics of Life Reviews,* 2**,** 157-175.

Peccoud, J. & Ycart, B. 1995. Markovian Modeling of Gene-Product Synthesis. *Theoretical Population Biology,* 48**,** 222-234.

Raj, A., Peskin, C. S., Tranchina, D., Vargas, D. Y. & Tyagi, S. 2006. Stochastic mRNA Synthesis in Mammalian Cells. *PLoS Biol,* 4**,** e309.

Raj, A. & van Oudenaarden, A. 2008. Nature, Nurture, or Chance: Stochastic Gene Expression and Its Consequences. *Cell,* 135**,** 216-226.

Schwanhäusser, B., Busse, D., Li, N., Dittmar, G., Schuchhardt, J., Wolf, J., Chen, W. & Selbach, M. 2011. Global quantification of mammalian gene expression control. *Nature,* 473**,** 337-342.

Starkie, R., Ostrowski, S. R., Jauffred, S., Febbraio, M. & Pedersen, B. K. 2003. Exercise and IL-6 infusion inhibit endotoxin-induced TNF-α production in humans. *The FASEB Journal,* 17**,** 884-886.

Stephens, M. A. 1974. EDF Statistics for Goodness of Fit and Some Comparisons. *Journal of the American Statistical Association,* 69**,** 730-737.

Wall, E. A., Zavzavadjian, J. R., Chang, M. S., Randhawa, B., Zhu, X., Hsueh, R. C., Liu, J., Driver, A., Bao, X. R., Sternweis, P. C., Simon, M. I. & Fraser, I. D. C. 2009. Suppression of LPS-Induced TNF-{alpha} Production in Macrophages by cAMP Is Mediated by PKA-AKAP95-p105. *Sci. Signal.,* 2**,** ra28-.